A Magnetic Resonance-Compatible Loading Device for Dynamically Imaging Shortening and Lengthening Muscle Contraction Mechanics

Amy Silder
Department of Biomedical Engineering,
University of Wisconsin–Madison,
Madison, WI 53706

Christopher J. Westphal
Department of Mechanical Engineering,
University of Wisconsin–Madison,
Madison, WI 53706

Darryl G. Thelen[1]
Department of Biomedical Engineering,
Department of Mechanical Engineering,
and Department of Orthopedics and Rehabilitation,
University of Wisconsin–Madison,
Madison, WI 53706
e-mail: thelen@engr.wisc.edu

The purpose of this study was to design and test a magnetic resonance (MR)-compatible device to induce either shortening or lengthening muscle contractions for use during dynamic MR imaging. The proposed device guides the knee through cyclic flexion-extension, while either elastic or inertial loads are imposed on the hamstrings. Ten subjects were tested in a motion capture laboratory to evaluate the repeatability of limb motion and imposed loads. Image data were subsequently obtained for all ten subjects using cine phase contrast imaging. Subjects achieved ~30 deg of knee joint motion, with individual subjects remaining within ~1 deg of their average motion across 56 repeated cycles. The maximum hamstring activity and loading occurred when the knee was flexed for the elastic loading condition (shortening contraction), and extended for the inertial loading condition (lengthening contraction). Repeat MR image acquisitions of the same loading condition resulted in similar tissue velocities, while spatial variations in velocity data were clearly different between loading conditions. The proposed device can enable dynamic imaging of the muscle under different types of loads, which has the potential to improve our understanding of basic muscle mechanics, identify potential causes of muscle injury, and provide a basis for quantitatively assessing injury effects at the tissue level. Slight modifications to the device design and/or subject positioning could allow for imaging of the quadriceps or the knee.
[DOI: 10.1115/1.3212559]

1 Introduction

Dynamic magnetic resonance (MR) imaging is a powerful approach for characterizing in vivo muscle mechanics. For example, studies showed that muscle fascicles and aponeurosis do not shorten uniformly [1,2], as commonly assumed in muscle models [3]. More recent techniques revealed a strong influence of musculotendon architecture on the spatial finite strain distributions within a contracting muscle [4,5]. Such information can be extremely helpful for improving the understanding of in vivo muscle function, for validating musculoskeletal models, and for critically evaluating the effects of clinical interventions.

MR-compatible limb loading devices have been successfully used during dynamic MR imaging to investigate shortening muscle contraction mechanics [1,6–8]. However, functional movement often involves active stretch-shortening cycles, during which the musculotendon lengthens under load, prior to shortening [9]. During the lengthening phase, muscle fibers can undergo an active lengthening contraction, which enhances force development but also makes the muscle more susceptible to injury [10]. Therefore, understanding in vivo tissue motion during lengthening contractions is relevant to understand both normal muscle function and potential injury mechanisms.

The goal of this study was to develop a MR-compatible device that can be used to impose either elastic or inertial loads on skeletal muscles, thereby inducing either shortening or lengthening contractions. The proposed device was designed to image the thigh or knee. Our initial focus is on the hamstrings, which is one of the most frequently injured muscles among athletes [11], and undergoes a stretch-shortening cycle during the late swing phase of running [12]. The primary challenge of this investigation was to generate sufficient inertial loads (proportional to mass*acceleration) within the physical constraints of a scanner and temporal constraints of dynamic MR pulse sequences. We address this issue by using a geared loading assembly to amplify the effective inertia felt by the limb during cyclic knee flexion-extension. In this paper, we describe the design of the device, and confirm that it induces repeatable motion, and the intended muscle contractions, which are both crucial for dynamic image acquisition and analysis. Preliminary data obtained from cine phase contrast (cine-PC) imaging are presented to demonstrate the effectiveness of the device during MR image acquisition.

2 Methods

2.1 Device Description. The device was designed to: (a) guide the limb through repeatable cyclic knee flexion-extension, while limiting thigh movement, (b) impose variable inertial or elastic loads on the hamstrings, (c) be constructed of nonferrous materials, resulting in the device being both MR safe and compatible [13], and (d) fit within the 60 cm bore of a standard MR scanner. Following is a description of the components of the device.

The base was made from 15.9 mm thick high density polyethylene (Fig. 1(*a*)). Ribs were designed to mimic the curvature of a GE 1.5 T MR scanner couch (General Electric Healthcare, Milwaukee, WI), and were secured to the underside of the base. The leg support assembly consists of a leg brace cross pinned to fixed uprights, which are aligned with the knee axis of rotation. Two arms extend from the uprights, on either side of the shank. These were thermoformed to curve inwards at the distal end, in order to minimize interference with the circular MR bore during maximum knee flexion. A 45-toothed sprocket was pinned to a shaft on the medial upright, which drives an acetal roller chain that connects the leg support assembly to the loading assembly.

The loading assembly consists of a gear box and a loading shaft located just distal to the foot (Fig. 1(*a*)). The roller chain drives a 12-toothed sprocket on an auxiliary brass shaft within the gear box. Two spur gears, located within the gear box, further amplify the motion of the knee. This results in an overall gear ratio of $N = 1$. Hence, the loading shaft rotates 10 deg for every 1 deg of knee rotation, and the equivalent inertia or spring stiffness felt by the subject is 100 ($1/N$ squared) times greater than the actual inertia or spring stiffness mounted on the loading shaft. Inertia disks (Fig. 1(*a*)) were constructed of solid surface material (density of 1574 kg/m^3, and thickness of 1.30 cm). Six disks of up to 22.2 cm in diameter can be used, allowing for the mass moment of inertia to be varied from 0 $kg\,cm^2$ to 288 $kg\,cm^2$ (equivalent inertia $0-2.88$ $kg\,m^2$) . Torsional springs (Fig. 1(*b*)) were con-

[1]Corresponding author.
Manuscript received May 8, 2009; final manuscript received July 29, 2009; published online September 3, 2009. Review conducted by Gerald E. Miller.

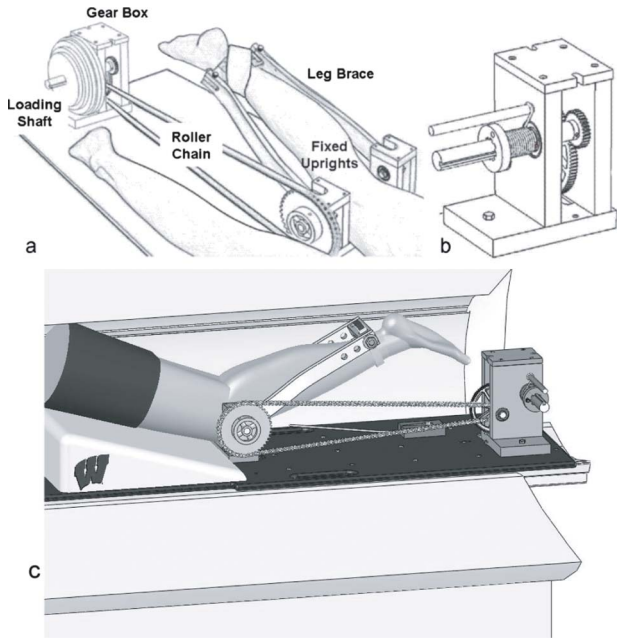

Fig. 1 (*a*) The subject lays prone on the base of the device with his/her knee joint aligned to an axis of rotation. A large sprocket and chain connect the externally applied loads to the knee. Further amplification of the loads, due to spur gears within the gear box, result in an overall gear ratio of 1:10. As a result, the equivalent inertia at the knee is 100 times greater than the inertia of the disks mounted on the loading shaft. (*b*) Alternatively, a torsional spring can be mounted on the loading shaft, thereby inducing an elastic load (i.e., shortening contraction). (*c*) The device fits securely within the bore of a scanner. The gear box is located at the far end of the base, such that the inertia disks and torsional spring can be interchanged without translating the couch between image sequence acquisitions.

structed of stainless steel wire (0.20 cm, 0.28 cm, and 0.32 cm in diameter, 10–13 turns per spring), allowing for stiffness values from 0 Nm/rad to 0.6 Nm/rad (equivalent stiffness 0–60 Nm/rad).

2.2 Loading Analysis. In use, subjects perform cyclic knee flexion-extension at a rate specified by a metronome. Assuming the motion is harmonic, the knee angle can be expressed as $\theta_k = A \sin \omega t + \bar{\theta}_k$, where t is the time in s, ω is the angular frequency in rad/s, $\bar{\theta}_k$ is the average knee angle, A is the amplitude of the motion, and $2A$ is the net knee excursion. The net internal knee flexion moment M_k can then be estimated as

$$M_k = \underbrace{-\left(I_s + \frac{I_d}{N^2}\right)\omega^2 A \sin \omega t}_{\text{inertial component}} + \underbrace{\frac{k}{N^2}(A \sin \omega t + \bar{\theta}_k)}_{\text{elastic component}} + m_s g \ell_s^* \cos(\theta_k - \theta_h) \quad (1)$$

where I_s is the moment of inertia of the foot, shank, and leg brace about the knee, m_s is the mass of the foot, shank, and leg brace, ℓ_s^* is the distance from the knee to the center of the mass of the combined leg and leg brace, I_d is the inertia of the disks, k is the torsional spring stiffness, θ_h is the hip angle, and N is the gear ratio (=0.1). Of note is that the inertial and elastic components are 180 deg out-of-phase. Thus, the torsional spring and inertial disks result in peak knee flexion moments when the knee is fully flexed and extended, respectively.

2.3 Experimental Testing. The limbs of 10 healthy volunteers were tested (6 females and 4 males, 32 ± 11 yrs of age, 1.75 ± 0.09 m in height, 70 ± 10 kg in weight). Subjects gave informed consent, according to a protocol approved by the University of Wisconsin's Health Sciences Institutional Review Board. Data were collected for each subject's right limb in a motion capture laboratory to evaluate the magnitude and repeatability of motion, loading, and induced muscle activities. Dynamic MR images were later obtained on each subject's same limb at the University of Wisconsin Hospital.

2.4 Motion Capture. Kinematic data were collected (100Hz) using an 8-camera passive motion capture system (Motion Analysis, Santa Rosa, CA). Knee flexion-extension angle was monitored using markers placed at the axis of rotation of the knee, and on support arms near the ankle. Two tensile load cells (FT24 tension load cells, Measurement Specialties, Hampton, VA) were attached within the top and bottom portions of the chain to provide a measurement of the chain tension. Electromyographic (EMG) signals were recorded (2000Hz) from the medial hamstrings using preamplified single differential surface electrodes (DE-2.1, DelSys, Inc., Boston, MA).

Subjects were positioned prone with the hip slightly flexed (~15 deg). Each subject performed the cyclic knee flexion-extension at 28 cycles per minute (cpm) to the beat of a metronome. A semicircular covering was used to emulate the physical constraints of a MR bore. Following adequate familiarization, subjects completed three 2 min trials, with at least 2 min rest for both loading conditions: elastic loading (k=0.4 Nm/rad) and inertial loading (I_d=2.02 kg cm^2). The order of loading conditions was randomized between subjects.

Knee angle and load cell data were digitally low-pass filtered at 6 Hz (fourth order bidirectional Butterworth filter). Anthropometric measures were used to estimate the mass and inertial properties of the lower leg for each subject [14]. Inverse dynamics analysis (with knee angle, angular acceleration, and load cell forces as inputs) was then used to estimate the net internal knee joint moment during motion.

Repeatability of the following measures was evaluated within and between trials: maximum and minimum knee angle, maximum net internal knee moment, and angle of peak knee moment. These measures were assessed using two-factor (loading condition, trial) repeated measures analysis of variance (ANOVA). Because dynamic image data are interpolated between the start and end of each flexion-extension cycle to produce the desired number of frames of motion, the cycle-to-cycle variability of the knee angle within each trial must be low. Accordingly, we quantified the standard deviation of the knee angle at 215 (~0.01 s sample interval) discrete points throughout the cyclic motion. The average of the 215 standard deviation values is reported in this manuscript.

EMG signals were full wave rectified and low-pass filtered at 6 Hz. Signals were normalized to the maximum signal observed across any of the six trials. The effect of the loading condition on muscle activity was assessed separately for the flexion and extension phases of motion. First, the mean knee angle for each flexion-extension cycle within each trial was found. The knee flexion phase was defined as any angle greater than the mean, and the knee extension phase was defined as any angle less than the mean. The average muscle activity during each phase was calculated for each cycle, and averaged across the entire trial. EMG activity was compared between loading conditions and the flexion and extension phases using paired t-tests.

Finally, each subject performed three consecutive isokinetic (30 deg/s) knee flexion-extension tasks using an isokinetic dynamometer (Biodex Multi-Joint System 2, Biodex Medical Systems, Inc.). This was done to gauge the magnitude of the induced loading relative to maximum effort.

2.5 Dynamic MR Imaging. Cine PC imaging was used to obtain tissue velocities for each subject. Three trials were conducted for each loading condition. Images were obtained in a sagittal-oblique plane for six subjects (Fig. 2(*a*)), and in a coronal-

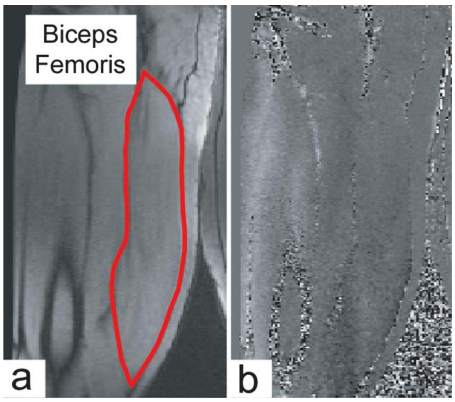

Fig. 2 (*a*) **A representative sagittal-oblique image, from which the data were obtained. The imaging plane was prescribed graphically using static localizer images. In this image, the subject is relaxed, with the knee in maximum extension.** (*b*) **Velocity images were obtained using cine phase contrast imaging. The gray scale represents the magnitude of the superior-inferior velocity for the elastic loading.**

oblique plane for four subjects. All scans were conducted on a GE 1.5 T MR scanner using a flex wrap coil. The imaging sequence was gated to the onset of knee flexion using a plethysmograph placed on the base of the device, under the ankle. Each scan lasted 1min 39 s, and resulted in one magnitude image and three velocity images per time frame. Scanning parameters were: voxel size $=1.4\times1.4\times6$ mm^3, encoding velocity=5 cm/s, 256×256 matrix, TR/TE=21.6/7.1 ms, two lines of *k*-space/cycle, 0.45 phase field of view, and 40 reconstructed frames/cycle. The image quality and hamstring tissue velocities were visually compared between subjects and across repeated trials of the same loading condition. Quantitative comparisons were made between loading conditions by assessing the regional variability in superior-inferior (SI) tissue velocity within the biceps femoris long head. This was done by first finding the mean and standard deviation of SI velocities within the biceps femoris long head at each of the 40 time frames. Regional variability was defined as the average standard deviation value across all 40 frames. The two-factor ANOVA was used to compare between trials and loading conditions.

3 Results

The device facilitated repeatable sinusoidal knee flexion-extension motion. Subjects achieved an average of 28.3 ± 4.7 deg of knee motion, and maintained a standard deviation within approximately 1 deg from their mean knee angle trajectory at each point throughout the flexion-extension cycle (a representative trial is given in Table 1). The maximum and minimum knee angle were also repeatable to within 1 deg, both within and across repeated trials, with no significant differences between loading conditions.

As predicted by the analytical model (Eq. (1)), the knee flexion moment due to the elastic and inertial loads were out of phase (Fig. 3). The peak knee flexion moment occurred, on average, within 1 deg of maximum knee extension for the inertial loading, and within 2 deg of maximum knee flexion for the elastic loading. The net joint moments induced about the knee were ~18 Nm for

Table 1 Measures obtained from one representative trial for each loading condition are presented. Less than 1 deg of variability was observed for both the maximum and minimum knee angle, as well as for the average standard deviation in the knee angle across 215 discrete points of the flexion-extension cycle. The loading conditions induced peak knee moments that were out of phase with each other, such that the peak loading occurred near maximum knee extension for the inertial loading, and near peak knee flexion for the elastic loading.

Subject	Loading	Average SD, knee angle (deg)	Maximum (SD) knee flexion angle (deg)	Minimum (SD) knee flexion angle (deg)	Angle (SD) of peak moment (deg)
1	Elastic	0.7	42.6(0.8)	16.6(0.6)	39.6(1.2)
	Inertia	0.6	42.6(0.8)	17.5(0.6)	17.8(1.4)
2	Elastic	0.7	42.2(0.7)	18.5(0.9)	41.3(0.3)
	Inertia	0.9	43.7(0.8)	18.5(0.6)	18.7(0.8)
3	Elastic	1.0	39.6(0.9)	18.4(1.0)	38.8(0.9)
	Inertia	0.7	39.4(1.1)	18.6(0.7)	17.9(0.3)
4	Elastic	0.9	46.5(0.9)	13.1(0.8)	43.9(3.0)
	Inertia	0.8	47.3(1.0)	15.4(0.5)	16.7(0.9)
5	Elastic	1.7	47.6(2.2)	15.5(1.2)	43.4(0.4)
	Inertia	1.4	49.0(1.8)	17.9(1.6)	18.0(1.2)
6	Elastic	0.7	41.3(1.0)	12.9(0.5)	40.2(0.2)
	Inertia	1.0	41.4(0.9)	14.0(0.6)	18.3(2.1)
7	Elastic	1.7	51.5(0.9)	15.7(0.5)	48.5(2.4)
	Inertia	1.6	51.3(0.9)	13.9(0.3)	14.3(0.9)
8	Elastic	2.2	47.4(1.4)	16.6(0.5)	46.4(1.7)
	Inertia	1.7	47.1(1.3)	17.2(0.9)	16.7(1.9)
9	Elastic	2.3	42.6(1.2)	16.2(0.7)	43.1(0.7)
	Inertia	1.4	41.1(0.9)	17.6(0.8)	17.7(1.2)
10	Elastic	1.4	39.7(0.5)	15.4(0.7)	37.2(1.7)
	Inertia	1.3	40.6(0.9)	13.4(0.4)	14.3(0.7)

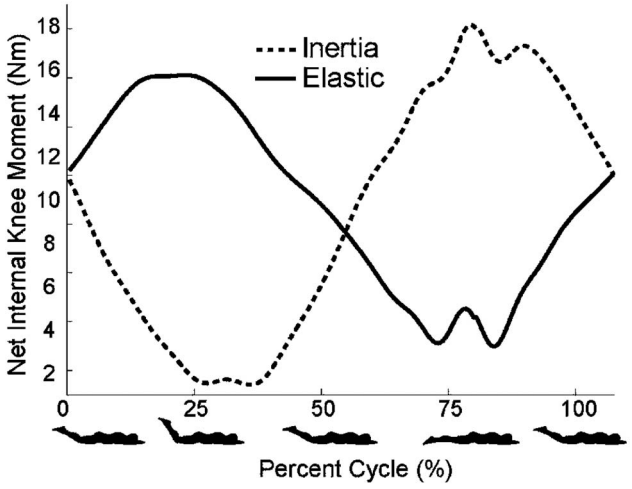

Fig. 3 The ensemble averaged net internal knee moments were out of phase between the elastic and inertial loading conditions. The maximum knee flexion moment occurred within 2 deg of peak knee flexion during the elastic loading, indicating that the muscle is undergoing a shortening contraction. In contrast, the maximum knee flexion moment occurred within 1 deg of peak knee extension for the inertial loading, indicating that the muscle is undergoing a lengthening contraction.

inertial loading, and ~16 Nm for the elastic loading. These loads ranged from 10% to 34% of each of the subject's maximum isokinetic knee flexion strength (89.7 ± 22.3 Nm).

The peak hamstring muscle activity corresponded closely with the angle of peak knee moment for both loading conditions. Specifically, significantly greater muscle activity occurred during the knee flexion phase for the elastic loading condition, and during the knee extension phase for the inertial loading condition (Fig. 4) ($p < 0.01$).

Finally, observations made during the dynamic MR imaging experiments confirmed that the device fit safely and securely on the couch and within the bore of the scanner (Fig. 1(*c*)). Images were obtained with no discernable distortions in the magnetic field

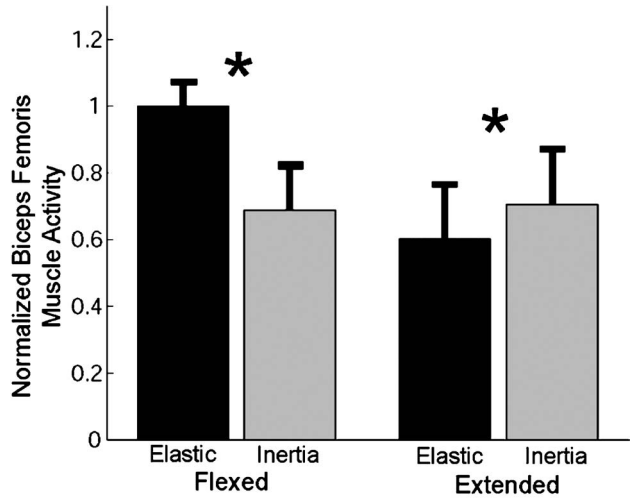

Fig. 4 Hamstring electromyographic measurements indicated that the device can be used to alter the timing of the hamstring activity between loading conditions. The mean hamstring activity was significantly greater (*$p < 0.5$) when the knee was flexed for the elastic loading, and when the knee was extended during the inertial loading condition.

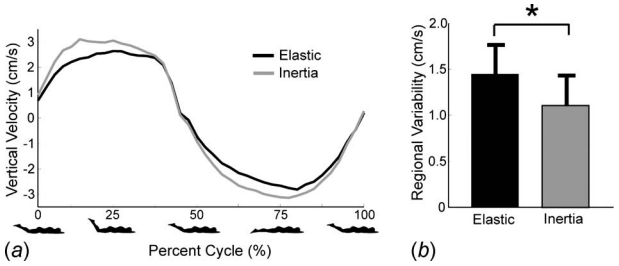

Fig. 5 (*a*) Shown are the ensemble averaged tissue velocities within the biceps femoris long head during the cyclic knee flexion-extension tasks. Mean tissue velocities within the muscle tissue were similar between loading conditions, with the inertial loading condition inducing slightly greater tissue velocities than the elastic loading condition. (*b*) Significantly (*$p < 0.5$) greater regional variability was present during the elastic loading condition, suggesting more nonuniform motion throughout the muscle tissue.

(Fig. 2). The torsional spring and inertial disks were interchanged on the device without repositioning the subject in the scanner, which is important to maintain a consistent imaging plane between loading conditions. The location of the plethysmograph resulted in clean pulses to trigger the start of each cycle. Repeated image acquisitions of the same loading condition resulted in similar tissue velocities, suggesting good repeatability of motion within the scanner. Ensemble averaged tissue velocities within the long head of the biceps femoris were similar between loading conditions, with the inertial loading condition inducing slightly greater peak velocities than the elastic condition (Fig. 5(*a*)). Both loads generated a sinusoidal pattern in tissue velocities characterizing the cyclic knee flexion-extension motion. Clear differences were observed between loading conditions with respect to the regional variability in vertical velocity measurements (Fig. 5(*b*)). Specifically, the elastic loading condition induced significantly greater variability in tissue velocities throughout the muscle, compared with the inertial loading ($p < 0.01$).

4 Discussion

The results obtained from our testing confirm that the MR-compatible device proposed is capable of inducing repeatable knee flexion-extension motion, and can be used during dynamic MR imaging. The use of a geared loading assembly with interchangeable inertial disks and a torsional spring allowed us to induce active lengthening and shortening hamstring muscle contractions within the bore of a standard MR scanner.

Various dynamic imaging sequences exist to visualize in-vivo muscle mechanics including velocity encoding, displacement encoding, and tagging [15,16]. In this study, we used cine PC, which encodes the three-dimensional velocity of each pixel in the phase of the signal [17]. Since the temporal location of the tissue is assumed to be the same within each flexion-extension cycle, inconsistent loading and/or motion would produce unreliable phase measurements, and thus, inaccurate velocity data. We used motion analysis techniques to test repeatability of both the loading and movement, and found that subjects were able to perform multiple flexion-extension cycles with low variability of motion (<1 deg) and angle of peak loading (~1–2 deg), both within and between trials. Because the device was designed to guide the limb through cyclic planar motion, it is feasible that slight modifications to the base size or support arms could help enable the imaging of children and/or individuals with pathologies.

The loads imposed on the limb were less than one-third of the maximum isokinetic knee flexion strength. Relatively low loads were used so as not to induce fatigue over the multiple cycles of motion required for cine PC imaging [17]. The device, as designed, is capable of imposing higher loads on the limb than used

in this study. In particular, the utilization of a 1:10 gear ratio greatly increased the loads experienced by the subject, while minimizing the size of the inertial disks and torsional springs needed. Thus, it is feasible to use the proposed device during a real time dynamic imaging sequence [18] to look at muscle contractions under larger loads. Such use is important for the assessment of potential injury mechanisms, which tend to occur with muscles near maximal activation and under large external loads [10].

The range of knee motion in the scanner was ~28 deg. This was limited by both the 60 cm bore diameter, as well as the length of the lower limb of the subject. As expected, the subjects with longer limbs had a smaller range of motion. Utilization of this device within a large bore scanner would increase the range of motion of the joint. Finally, having the loading assembly located on the far end of the device allows the type and/or magnitude of load to be changed between image acquisitions without moving the subject. This feature is important for retaining a constant imaging plane for different loading conditions.

Visual inspection of the images revealed clear differences between loading conditions, with the proximal muscle tissue exhibiting larger superior-inferior velocity in the elastic condition. These results were confirmed by assessing the average standard deviation of vertical velocities across all 40 frames, defined as the regional variability. The elastic loading induced significantly greater regional variability in velocity data, compared with the inertial loading condition. An important avenue of future research is to numerically integrate the velocity data to estimate displacement and strain deformation patterns within the muscle tissue. New techniques are emerging to perform such analyses [5,16], which, when coupled with images obtained using the proposed device, could facilitate the empirical analysis of lengthening contraction mechanics. This is important to better understand potential injury mechanisms and the effect of muscle remodeling on in vivo mechanics following injury [19] or surgical procedures [20]. Finally, while the proposed device was tested for hamstring imaging, repositioning of the subject and/or the use of alternative coils make imaging of the knee joint or quadriceps muscles directly feasible.

Acknowledgment

We would like to thank Eric Bader for his effort in the initial design of the device, and the support provided by the National Institutes of Health (R01 AR56201), National Football League Charities, the Tong Family Foundation, a National Science Foundation Pre-doctoral Fellowship (AS), and an American Society of Biomechanics Grant-In-Aid (AS). We would also like to thank Silvia Blemker, Ph.D., and Scott Reeder, MD, Ph.D., for their help with MRI protocol development and image analysis.

References

[1] Pappas, G. P., Asakawa, D. S., Delp, S. L., Zajac, F. E., and Drace, J. E., 2002, "Nonuniform Shortening in the Biceps Brachii During Elbow Flexion," J. Appl. Physiol., **92**(6), pp. 2381–2389.
[2] Finni, T., Hodgson, J. A., Lai, A. M., Edgerton, V. R., and Sinha, S., 2003, "Nonuniform Strain of Human Soleus Aponeurosis-Tendon Complex During Submaximal Voluntary Contractions In Vivo," J. Appl. Physiol., **95**(2), pp. 829–837.
[3] Zajac, F. E., 1989, "Muscle and Tendon: Properties, Models, Scaling, and Application to Biomechanics and Motor Control," Crit. Rev. Biomed. Eng., **17**(4), pp. 359–411.
[4] Zhong, X., Epstein, F. H., Spottiswoode, B. S., Helm, P. A., and Blemker, S. S., 2008, "Imaging Two-Dimensional Displacements and Strains in Skeletal Muscle During Joint Motion by Cine DENSE MR," J. Biomech., **41**(3), pp. 532–540.
[5] Zhou, H., and Novotny, J. E., 2007, "Cine Phase Contrast MRI to Measure Continuum Lagrangian Finite Strain Fields in Contracting Skeletal Muscle," J. Magn. Reson Imaging, **25**(1), pp. 175–184.
[6] Asakawa, D. S., Pappas, G. P., Blemker, S. S., Drace, J. E., and Delp, S. L., 2003, "Cine Phase-Contrast Magnetic Resonance Imaging as a Tool for Quantification of Skeletal Muscle Motion," Semin. Musculoskelet. Radiol., **7**(4), pp. 287–295.
[7] Drace, J. E., and Pelc, N. J., 1994, "Skeletal Muscle Contraction: Analysis With Use of Velocity Distributions From Phase-Contrast MR Imaging," Radiology, **193**(2), pp. 423–429.
[8] Hidler, J., Hodics, T., Xu, B., Dobkin, B., and Cohen, L. G., 2006, "MR Compatible Force Sensing System for Real-Time Monitoring of Wrist Moments During FMRI Testing," J. Neurosci. Methods, **155**(2), pp. 300–307.
[9] Komi, P. V., 1984, "Physiological and Biomechanical Correlates of Muscle Function: Effects of Muscle Structure and Stretch-Shortening Cycle on Force and Speed," Exerc Sport Sci. Rev., **12**, pp. 81–122.
[10] Lieber, R. L., and Friden, J., 2002, "Mechanisms of Muscle Injury Gleaned From Animal Models," Am. J. Phys. Med. Rehabil., **81**(11), pp. S70–S79.
[11] Noonan, T. J., and Garrett, W. E., Jr., 1999, "Muscle Strain Injury: Diagnosis and Treatment," J. Am. Acad. Orthop. Surg., **7**(4), pp. 262–269.
[12] Thelen, D. G., Chumanov, E. S., Sherry, M. A., and Heiderscheit, B. C., 2006, "Neuromusculoskeletal Models Provide Insights Into the Mechanisms and Rehabilitation of Hamstring Strains," Exerc Sport Sci. Rev., **34**(3), pp. 135–141.
[13] Shellock, F. G., 2002, "Magnetic Resonance Safety Update 2002: Implants and Devices," J. Magn. Reson Imaging, **16**(5), pp. 485–496.
[14] Hoy, M. G., Zajac, F. E., and Gordon, M. E., 1990, "A Musculoskeletal Model of the Human Lower Extremity: The Effect of Muscle, Tendon, and Moment Arm on the Moment-Angle Relationship of Musculotendon Actuators at the Hip, Knee, and Ankle," J. Biomech., **23**(2), pp. 157–169.
[15] Aletras, A. H., Ding, S., Balaban, R. S., and Wen, H., 1999, "DENSE: Displacement Encoding With Stimulated Echoes in Cardiac Functional MRI," J. Magn. Reson., **137**(1), pp. 247–252.
[16] Zhu, Y., Drangova, M., and Pelc, N. J., 1997, "Estimation of Deformation Gradient and Strain From Cine-PC Velocity Data," IEEE Trans. Med. Imaging, **16**(6), pp. 840–851.
[17] Drace, J. E., and Pelc, N. J., 1994, "Measurement of Skeletal Muscle Motion In Vivo With Phase-Contrast MR Imaging," J. Magn. Reson Imaging, **4**, pp. 157–163.
[18] Asakawa, D. S., Nayak, K. S., Blemker, S. S., Delp, S. L., Pauly, J. M., Nishimura, D. G., and Gold, G. E., 2003, "Real-Time Imaging of Skeletal Muscle Velocity," J. Magn. Reson Imaging, **18**(6), pp. 734–739.
[19] Silder, A., Heiderscheit, B. C., Thelen, D. G., Enright, T., and Tuite, M. J., 2008, "MR Observations of Long-Term Musculotendon Remodeling Following a Hamstring Strain Injury," Skeletal Radiol., **37**(12), pp. 1101–1109.
[20] Asakawa, D. S., Blemker, S. S., Gold, G. E., and Delp, S. L., 2006, "Dynamic Magnetic Resonance Imaging of Muscle Function After Surgery," Skeletal Radiol., **35**(12), pp. 885–886.